A Five-Phase Reluctance Motor with High Specific Torque

Hamid A. Toliyat, Longya Xu, and Thomas A. Lipo, *Fellow, IEEE*

Abstract—**An alternative topology for a synchronous reluctance motor (SRM) is proposed utilizing a novel five-phase, concentrated winding, wye-connected stator. The corresponding inverter requires only 10 transistors, each of which operate at a better switch utilization factor than a conventional three-phase, six-transistor bridge. It is shown that this machine is capable of producing about 10% more torque per rms current flowing through winding than the normal three-phase SRM.**

Introduction

As THE WORKHORSE of industry, the prominence of the induction motor remains secure. Recently, however, improved types of permanent-magnet and reluctance motors have prompted a revival of interest in such machines. In particular, the so-called switched-reluctance [1] or variable-reluctance motor [2] has attracted much attention. This type of machine is a doubly salient structure having projecting poles on both the stator and the rotor. By winding and sequentially exciting coils around the stator poles, reluctance torque is produced between adjacent poles. Another type of machine receiving increased attention is the synchronous reluctance motor (SRM) [3], [4], which has also had a long history [5]. In this case, the rotor retains saliency, but the stator consists of a conventional cylindrical structure. It has been shown that this type of machine competes favorably with the variable-reluctance motor when the saliency ratio of the machine reaches 5:1. Machines possessing this degree of saliency and greater have already been reported [6], [7].

In the past, SRM's were excited with sinusoidal voltages, which in turn produced sinusoidal currents that produced a spatial MMF with respect to the rotor poles, which varied with load. As a result, these machines typically operated at a poor power factor. With the advent of solid-state power converters, it is now possible to excite the machine not only with sinusoidal waveforms producing an MMF of any desirable spatial position with respect to the rotor poles but also of current waveforms of any desirable waveshape. In particular, it has been shown that the use of a two-phase machine employing unidirectional square wave currents in concentrated windings results in a variable-speed drive that utilizes only two transistors in the associated power converter [3].

Paper IPCSD 91-105, approved by the Electric Machines Committee of the IEEE Industry Applications Society for presentation at the 1990 Industry Applications Society Annual Meeting, Seattle, WA, October 7-12. This work was supported by the Wisconsin Electric Machines and Power Electronics Consortium (WEMPEC) of the University of Wisconsin-Madison. Manuscript released for publication June 25, 1991.

The authors are with the Department of Electrical and Computer Engineering, University of Wisconsin-Madison, Madison, WI 53705

IEEE Log Number 9106829.

In a recent paper [4], it was shown that a third harmonic can be added to the fundamental component to help the spatial MMF to a peaked waveform, which results in an increased torque per rms ampere. Unfortunately, the machine employed in [4] was a dual three-phase machine having six isolated windings. The associated frequency converter was comprised of six single-phase bridges necessitating the use of a minimum of 16 and as many as 24 solid-state switching devices depending on the topology (which is not discussed in this paper).

Although a three-phase, three-wire system cannot support a third harmonic component of current, third harmonics can, however, flow in systems having a different number of phases. In particular, five-phase systems are particularly attractive since they require the fewest number of transistors beyond a three-phase system. The performance of such a five-phase reluctance motor excited with an optimized current waveform is the subject of this paper.

Linear Analysis

Fig. 1 shows a SRM with elementary two-pole, five-phase, full-pitch, concentrated windings that are 72° displaced in space. The winding function [8] for a typical phase is given in Fig. 2. Fig. 3 illustrates an idealized representation of the inverse gap function in which the flux is assumed to be only radially directed. The spatial MMF pattern at any instant resulting from the coil currents is determined by the product of instantaneous currents in all the coils and their corresponding winding functions. The rotational movement of the pattern with time is decided by the time variation of these currents, i.e., the current waveforms. Fig. 4 shows a five-phase inverter that can be used to generate both fundamental and third-harmonic-current components in the motor windings by means of pulse-width modulation (PWM). In general, with five phases, the following current waveforms can be assumed:

$$
\begin{aligned}
i_a &= \sqrt{2}\left[I_1 \sin\theta + I_3 \sin 3\theta\right] \\
i_b &= \sqrt{2}\left[I_1 \sin\left(\theta - \frac{2\pi}{5}\right) + I_3 \sin 3\left(\theta - \frac{2\pi}{5}\right)\right] \\
i_c &= \sqrt{2}\left[I_1 \sin\left(\theta - \frac{4\pi}{5}\right) + I_3 \sin 3\left(\theta - \frac{4\pi}{5}\right)\right] \\
i_d &= \sqrt{2}\left[I_1 \sin\left(\theta + \frac{4\pi}{5}\right) + I_3 \sin 3\left(\theta + \frac{4\pi}{5}\right)\right] \\
i_e &= \sqrt{2}\left[I_1 \sin\left(\theta + \frac{2\pi}{5}\right) + I_3 \sin 3\left(\theta + \frac{2\pi}{5}\right)\right]. \qquad (1)
\end{aligned}
$$

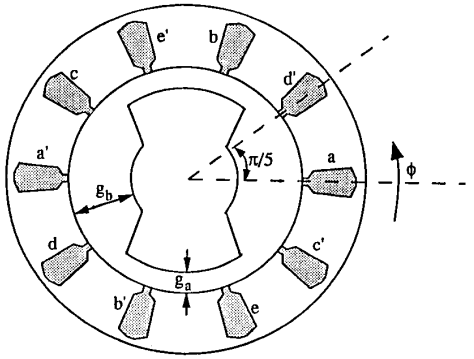

Fig. 1. Synchronous reluctance motor with two-pole, five-phase concentrated windings.

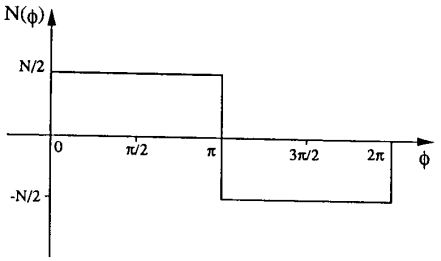

Fig. 2. Winding function for each phase of five-phase SRM.

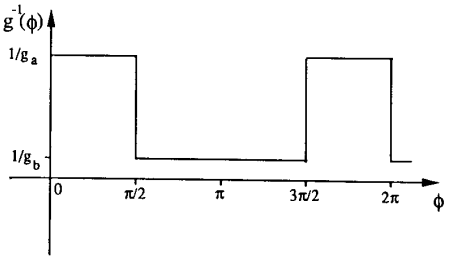

Fig. 3. Air-gap function for a SRM.

The spatial MMF pattern and its fundamental component corresponding to five-phase excitation is shown in Fig. 5 with $I_3 = 0$. When the windings are excited only with a fundamental and no third harmonic, this type of excitation is termed *Type I excitation*. Fig. 6 shows the spatial MMF and its fundamental if only the third harmonic of the current waveforms is applied. Finally, in Fig. 7, the resulting MMF waveform produced by both the fundamental and a typical third harmonic current (*Type II excitation*) is shown. The corresponding current waveform of one phase is shown in Fig. 8. Again, both the exact form of the MMF as well as the combination of the first and third harmonic components are plotted. Note that the peak MMF has been increased, which will be later shown to increase the resultant torque per ampere ratio.

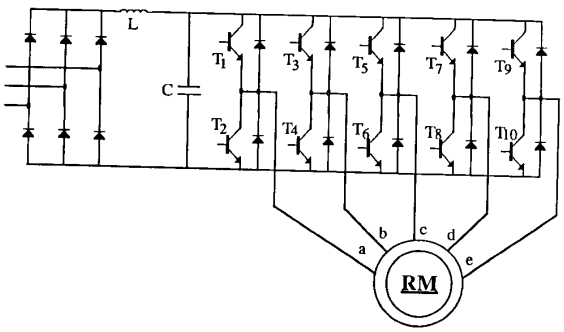

Fig. 4. Five-phase current regulated PWM.

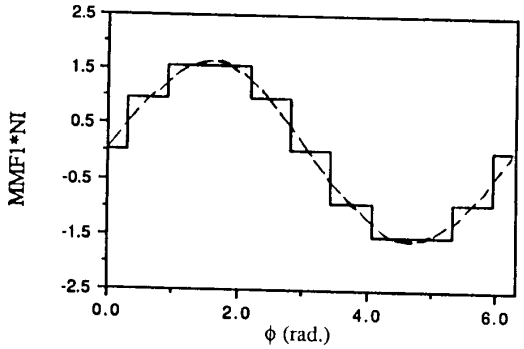

Fig. 5. Spatial MMF pattern and its fundamental if only the fundamental of the current waveform is applied.

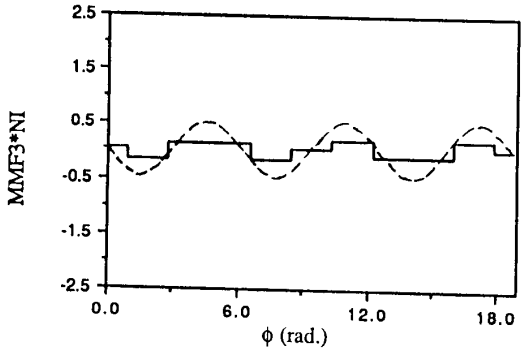

Fig. 6. Spatial MMF and its third harmonic if only the third harmonic of the current waveform is applied.

Reluctance Motor Torque Analysis

In this section, the air-gap torque of a SRM containing both first and third spatial harmonics [4], [9] is presented. It is assumed that iron is infinitely permeable, and the effect of saturation, tooth harmonics, and fringing are neglected. The current loading, which is the effective amperes per meter of periphery, can then be represented by

$$\Delta = \frac{2mPN_pIK_pK_d}{\pi D} \tag{2}$$

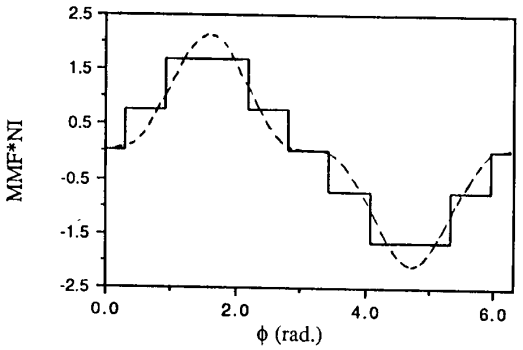

Fig. 7. Resulting MMF waveform produced by both a fundamental and third-harmonic current component.

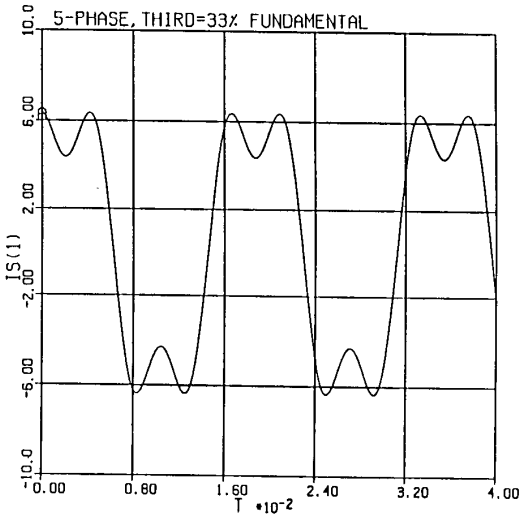

Fig. 8. Input current waveform illustrating an addition of third harmonic of current equal to 33% of the fundamental.

where D is the stator inner diameter, N_p is the number of turns per pole per phase, I is the rms current in each phase, and K_p and K_d are pitch and distribution factors respectively. Equation (3) gives the peak of the air-gap fundamental MMF wave of a P-pole, m-phase winding:

$$F_1 = \frac{\sqrt{2}\, D \Delta_1}{P}. \tag{3}$$

Similarly, the peak of air-gap third harmonic MMF wave is given by

$$F_3 = \frac{\sqrt{2}\, D \Delta_3}{3P}. \tag{4}$$

The air-gap flux density under the pole is given by

$$B = \frac{\mu_0}{g_a} F \tag{5}$$

where g_a is the air-gap under the pole and μ_0 is the permeability of free space. The resultant MMF due to the first and third harmonic is given by

$$F = F_1 \sin \varphi - F_3 \sin 3\varphi. \tag{6}$$

In the ideal case neglecting the tangential component of the air-gap flux density, flux in the airgap is radial and only exists under the pole arc. Therefore, the ideal energy in the airgap under the pole, shown in Fig. 9 , is

$$W_f = \frac{DLg_a^P}{4\mu_0} \int_{\frac{\pi}{2} - \frac{\tau_p}{2} - \alpha}^{\frac{\pi}{2} + \frac{\tau_p}{2} - \alpha} B^2 \, d\varphi. \tag{7}$$

Assuming that iron is not saturated, energy and coenergy are equal, and therefore, the derivative of this quantity with respect to α gives the torque

$$T_e = k \left\{ \left(\frac{F_1^2}{2} + F_1 F_3 \right) \left[\cos(\tau_p + 2\alpha) - \cos(\tau_p - 2\alpha) \right] + F_1 F_3 \left[\cos(2\tau_p + 4\alpha) - \cos(2\tau_p - 4\alpha) \right] + \frac{F_3^2}{2} \left[\cos(3\tau_p + 6\alpha) - \cos(3\tau_p - 6\alpha) \right] \right\} \tag{8}$$

where

$$k = \frac{\mu_0 DLP}{4 g_a}.$$

It is possible to use (8) to evaluate the effect of the addition of the third harmonic as well as the variation of pole arc τ_p as well as current angle α. Using the following minimization criteria

$$\min.\{-T\}$$

$$\text{s.t. } 0 < \alpha < \frac{\pi}{2}$$

$$0 < \tau_p < \pi$$

$$I_1^2 + I_3^2 = I^2$$

it was determined that a 90° pole arc and 45° current angle are the optimum values. The optimum amount of third harmonic required was about 33% of the fundamental current. Fig. 10 shows the variation of torque with respect to the amount of third harmonic added as well as current angle.

Winding Function Approach

In this section, the winding function approach is used to find the electromagnetic torque and the input voltages. Again, it is assumed that the iron is linear, stator windings are identical with axes of symmetry, and that eddy current, friction, and windage losses are neglected.

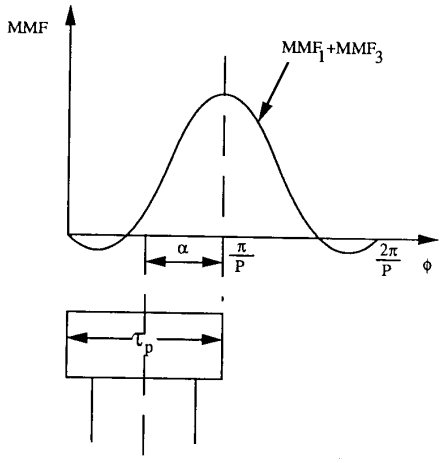

Fig. 9. Air-gap MMF with respect to the pole arc.

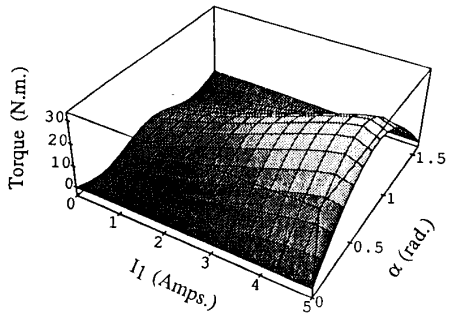

Fig. 10. Variation of torque with current angle and fundamental component of stator current when third harmonic is added for 90° pole arc.

Stator Voltage Equations

The voltage equations for the stator windings can be written

$$V_s = [R_s] I_s + \frac{d\Lambda_s}{dt} \tag{9}$$

where the vectors V_s, I_s, and Λ_s are defined by

$$\Lambda_s = [L_{ss}] I_s \tag{10}$$

and

$$I_s = [i_a^s \quad i_b^s \quad \cdots \quad i_e^s]^t \tag{11}$$

$$V_s = [v_a^s \quad v_b^s \quad \cdots \quad v_e^s]^t \tag{12}$$

and "t" denotes the transpose. The matrix $[R_s]$ is a 5 by 5 matrix given by

$$[R_s] = r_s[I] \tag{13}$$

where the matrix $[I]$ is a 5 by 5 identity matrix, and r_s is the resistance of each coil, assuming all coils are similar.

Due to conservation of energy, the inductance matrix $[L_{ss}]$ is a symmetric 5 by 5 matrix of the form

$$[L_{ss}] = \begin{bmatrix} L_{aa}^s & L_{ab}^s & \cdots & L_{ae}^s \\ L_{ba}^s & L_{bb}^s & \cdots & L_{be}^s \\ & & \cdots & \vdots \\ \vdots & \vdots & \cdots & \\ L_{ea}^s & L_{eb}^s & \cdots & L_{ee}^s \end{bmatrix}. \tag{14}$$

Since the inductance matrix $[L_{ss}]$ varies with the position of the rotor, the second term of (9) can be written as

$$\frac{d\Lambda_s}{dt} = [L_{ss}] \frac{dI_s}{dt} + \frac{d[L_{ss}]}{dt} I_s. \tag{15}$$

The second term in the above equation can be written using the chain rule as

$$\frac{d[L_{ss}]}{dt} I_s = \frac{d[L_{ss}]}{d\theta_r} \frac{d\theta_r}{dt} I_s. \tag{16}$$

Defining equivalent rotor electrical speed as

$$\omega_r = \frac{d\theta_r}{dt} \tag{17}$$

then

$$\frac{d\Lambda_s}{dt} = [L_{ss}] \frac{dI_s}{dt} + \omega_r \frac{d[L_{ss}]}{d\theta_r} I_s. \tag{18}$$

Torque Equation

The electrical torque can be found from the magnetic coenergy W_{co}

$$T_e = \left(\frac{\partial W_{co}}{\partial \theta_r} \right)_{(I_s \text{ constant})}. \tag{19}$$

In a linear magnetic system, the coenergy is equal to the stored magnetic energy

$$W_{co} = \frac{1}{2} I_s^t [L_{ss}] I_s. \tag{20}$$

From (19)-(20), considering the fact that the self inductance of each coil is constant results in

$$\begin{aligned} T_e = {} & \frac{dL_{ab}}{d\theta_r} i_a i_b + \frac{dL_{ac}}{d\theta_r} i_a i_c + \frac{dL_{ad}}{d\theta_r} i_a i_d + \frac{dL_{ae}}{d\theta_r} i_a i_e \\ & + \frac{dL_{bc}}{d\theta_r} i_b i_c + \frac{dL_{bd}}{d\theta_r} i_b i_d + \frac{dL_{be}}{d\theta_r} i_b i_e + \frac{dL_{cd}}{d\theta_r} i_c i_d \\ & + \frac{dL_{ce}}{d\theta_r} i_c i_e + \frac{dL_{de}}{d\theta_r} i_d i_e. \end{aligned} \tag{21}$$

The mutual inductance variation using the method presented in [8] is depicted in Fig. 11.

In order to demonstrate the potential improvement obtained by injection of a third-harmonic current, the above-mentioned approach has been used to simulate a five-phase

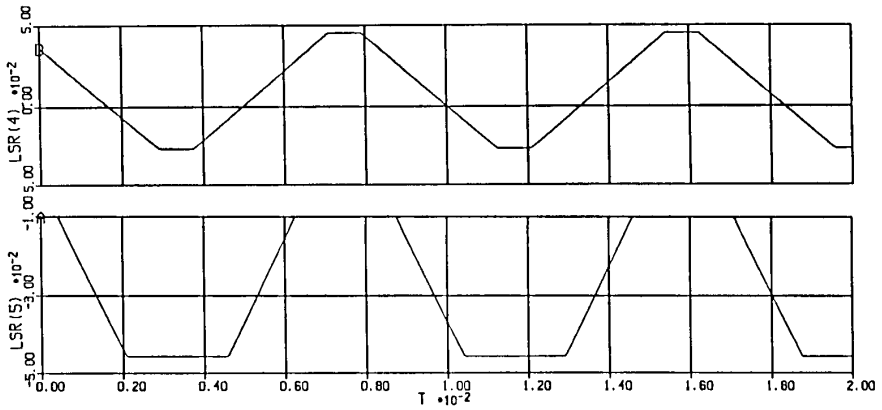

Fig. 11. Variation of mutual inductances with the rotor position.

SRM using the digital computer. The machine is assumed to have 40 stator slots and eight poles. Fig. 12(a) portrays the instantaneous electromagnetic torque when only the fundamental current waveform is applied (Type I excitation). The effect of the teeth in torque ripple is exaggerated by sharp edges in modeling, and the winding functions is clear. Fig. 12(b) presents the torque when a third-harmonic component equal to 33% of fundamental is added to the current (Type II excitation). A rather high torque pulsation due to the third-harmonic injection is obvious. However, these pulsations are filtered by the rotor mechanical inertia. It is important to keep in mind that in this study, the total rms current in all cases are maintained the same. Fig. 13 illustrates the variation of electromagnetic torque with the current angle α (angle of the stator current phasor with respect to the quadrature axis). It can be noted that a 14% increase in torque at $\alpha = 45°$ is obtained, compared with the case without third-harmonic current.

Nonlinear Analysis

It is clear that the linear model that has been presented has provided needed insight into determining the principles of the torque production in a five-phase SRM when excited with both fundamental and third-harmonic components of current. However, to properly evaluate and compare the design and performance of a five-phase SRM, more reliable models are required. For this purpose, the magnetic field of the machine under study was modeled in a discretized fashion and solved by a finite-element method package [10]. The machine has the same specifications as given in the linear case. In order to evaluate the torque capability in terms of rate of coenergy variation with respect to the rotor position, field plots for numerous different rotor positions were obtained.

Figs. 14 and 15 show vector potential lines (flux lines) for a typical rotor positions for the Type I (no third harmonic) and Type II (fundamental plus third harmonic) SRM's, respectively. These plots provide a good descriptive picture of flux distribution. In addition, those points of local saturation can be spotted easily by inspection. It was previously pointed out that the MMF produced by the stator tends to have

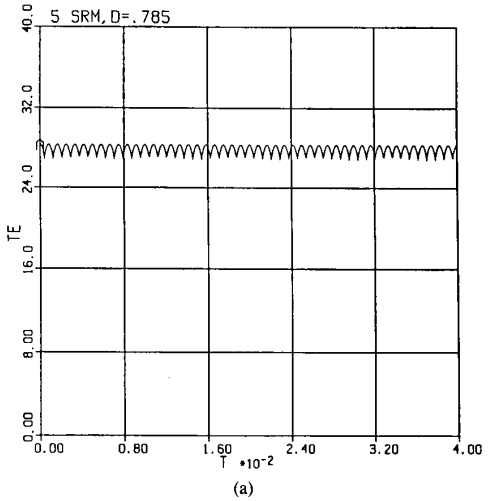

(a)

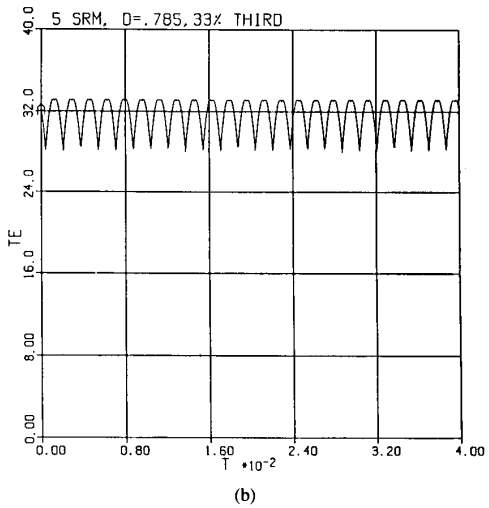

(b)

Fig. 12. (a) Instantaneous electromagnetic torque waveform of five-phase SRM with only fundamental current waveform applied; (b) instantaneous electromagnetic torque waveform of five-phase SRM with addition of 33% third harmonic of current.

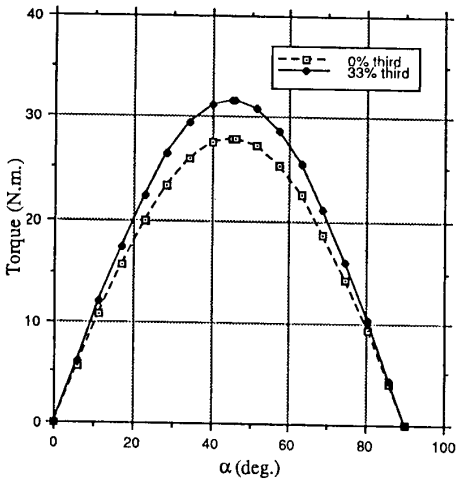

Fig. 13. Torque versus current angle α.

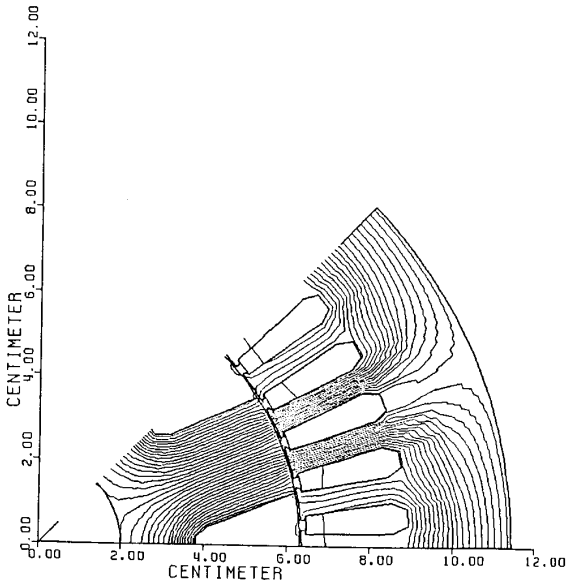

Fig. 14. Vector potential lines for Type I excitation for $\alpha = 18°$.

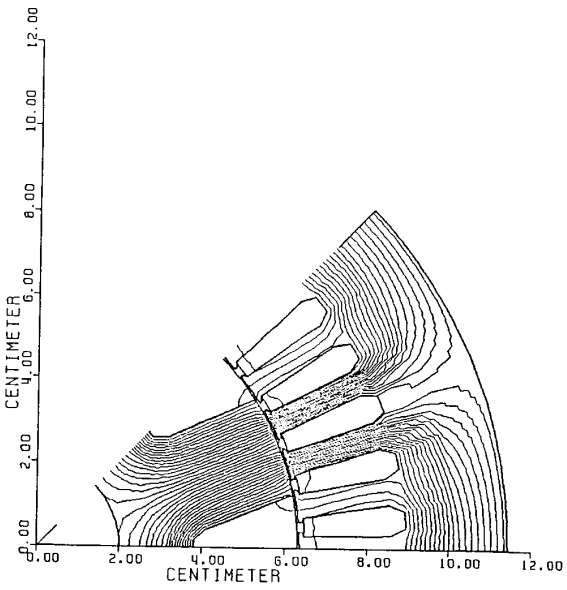

Fig. 15. Vector potential lines for Type II excitation for $\alpha = 18°$.

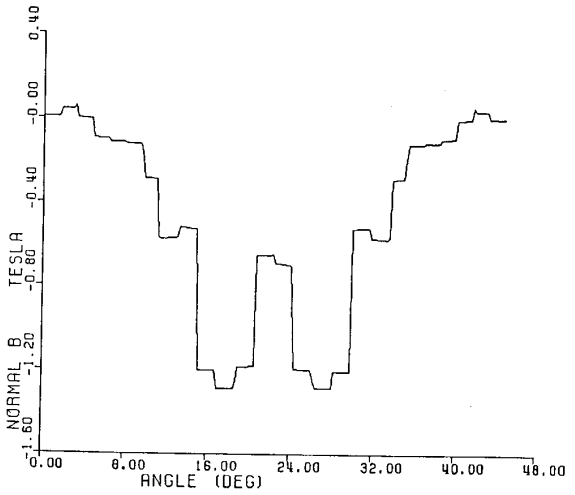

Fig. 16. Flux density in the air gap for Type I excitation for $\alpha = 18°$.

peaked waveshape in Type II excitation, and as a result, the flux density in the airgap is greater than for Type I excitation. This conclusion is clear from comparison of Figs. 16 and 17.

Figs. 18 and 19 show the flux density in the stator teeth. Again, because of the peaked MMF waveshape in the airgap, the flux density for the Type II excitation is higher than for the Type I. However, the flux density in the stator core depicted in Figs. 20 and 21 show a higher value for Type I than Type II. The reason is that the flux density in the back iron is the integral of flux density in the teeth. This reduced flux density enables the design of deeper slots in the stator and consequently allows for more space for copper on the stator side.

The average torque production is evaluated by calculating the rate of coenergy variation due to the rotor rotation, that is

$$T_e = \left(\frac{\Delta W_{co}}{\Delta \theta_{rm}}\right) I = \text{const.} \tag{22}$$

where ΔW_{co} is the coenergy variation corresponding to the variation of rotor angle displacement $\Delta \theta_{rm}$ in mechanical degrees under constant excitation current. Fig. 22 illustrates the variation of coenergy with the rotor position. Since the coenergy variations as it is clear are smooth, it is therefore

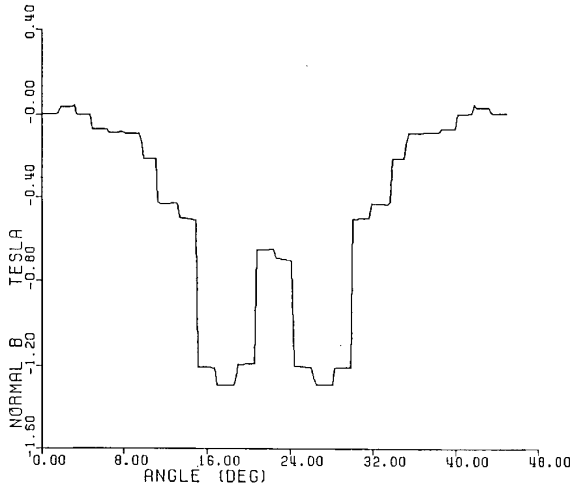

Fig. 17. Flux density in the air gap for Type II excitation for $\alpha = 18°$.

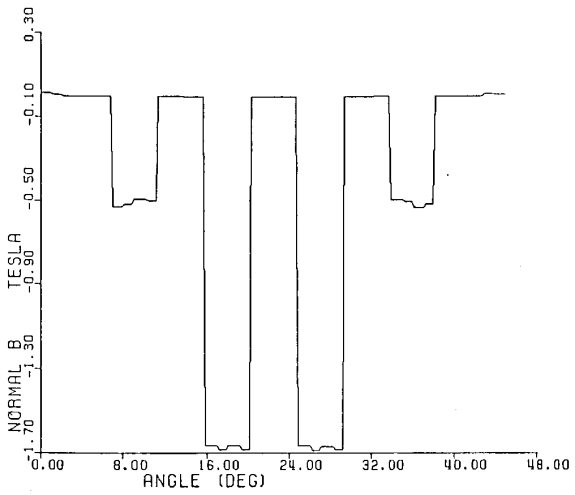

Fig. 18. Flux density in the stator teeth for Type I excitation for $\alpha = 18°$.

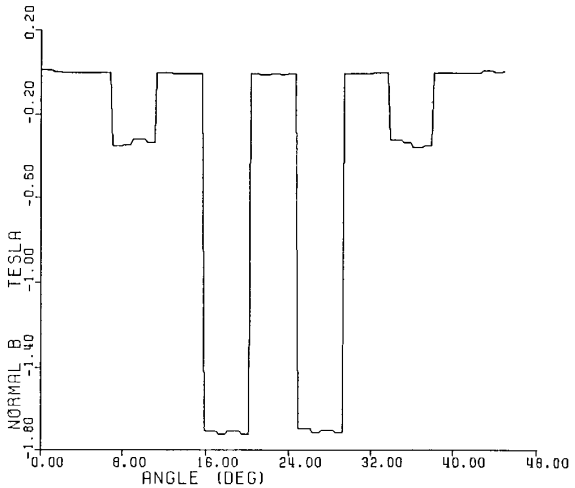

Fig. 19. Flux density in the stator teeth for Type II excitation for $\alpha = 18°$.

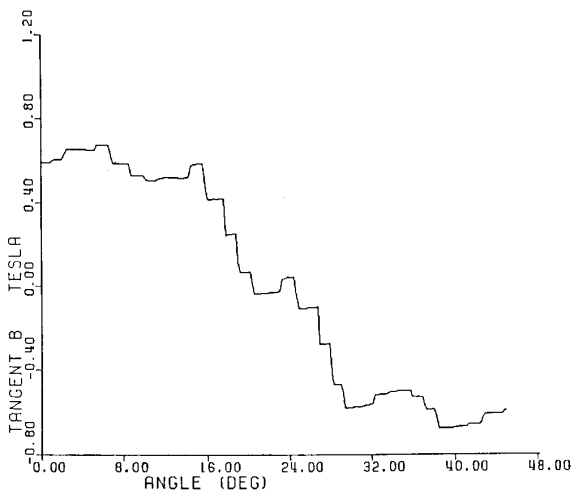

Fig. 20. Flux density in the stator core for Type I excitation of $\alpha = 18°$.

possible to fit them into fifth-order polynomials. The derivative of these fifth-order polynomials can be used to calculate the electromagnetic torque, which are depicted in Fig. 23. Note that at least a 10% improvement remains in the developed torque compared with the 14% improvement for the linear case of Fig. 13. It is apparent that the saturation of reluctance motors is crucial to the overall performance of such machines.

Experimental Results

The five-phase SRM designed and fabricated is a standard frame of a 7.5-hp, four-pole, 60-Hz, 460-V, three-phase, 36-stator slot, 28-rotor bar induction motor. However, the stator of the five-phase machine has 40 slots. The machine is wound with full-pitch single-layer coils and has four poles, which results in two slots per pole per phase. The salient pole rotor was milled from the corresponding three-phase squirrel-cage induction motor. Half of the pole pitch area for each pole was milled away to resemble the 90-electrical-degree pole arc achieved in the previous analysis.

The five-phase current-regulated PWM inverter using IGBT's as the switching devices and Motorola DSP56000 with the corresponding analog and digital hardwares were fabricated in the lab. Since the inverter has a rather high switching frequency, the stator currents of the motor can be rapidly adjusted in magnitude and phase. Fig. 24 is a typical trace illustrating the stator current under no-load operation.

To compare the torque capability of the motor under sinusoidal and the combined fundamental and third-harmonic excitations, a locked rotor test was carried out. The shaft of the motor was locked using a locking device. Next, the dc values of the sinusoidal currents at one instant of time was applied. The shaft was moved incrementally, and the steady-state torque was recorded using a digital torque meter. A

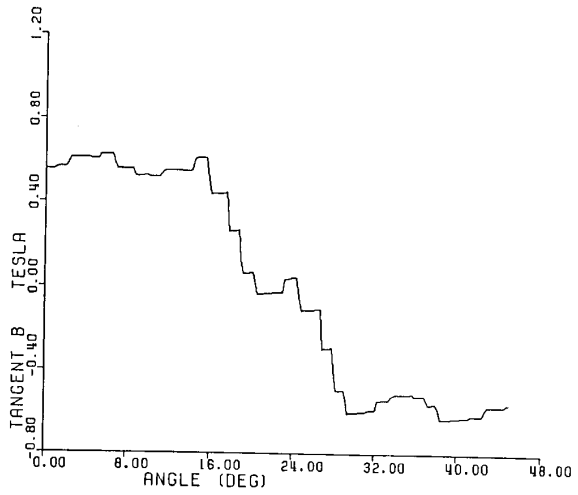

Fig. 21. Flux density in the stator core for Type II excitation for $\alpha = 18°$.

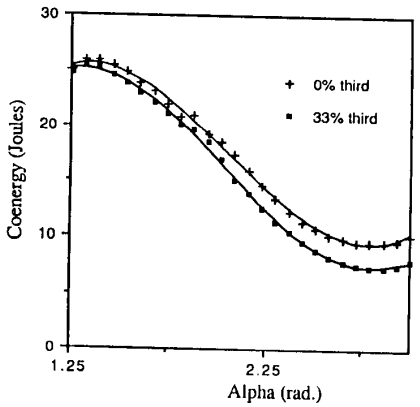

Fig. 22. Variation of coenergy with current angle (α).

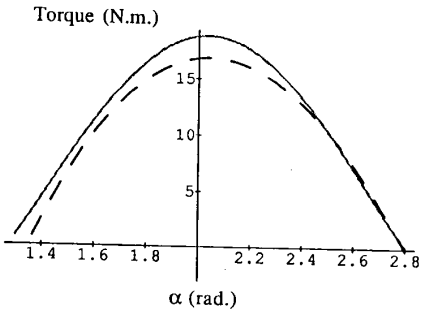

Fig. 23. Variation of electromagnetic torque with current angle (α).

similar test was carried out for the combined fundamental and third-harmonic injection. In both cases, the stator rms current was kept the same. Fig. 25 demonstrates variation of the shaft torque with respect to rotor position. A marked improvement in torque performance is clearly evident.

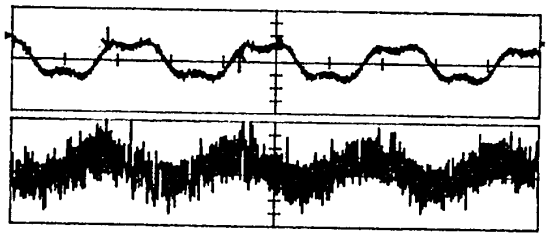

Fig. 24. Experimental trace of stator current waveform under combined fundamental and third-harmonic excitation.

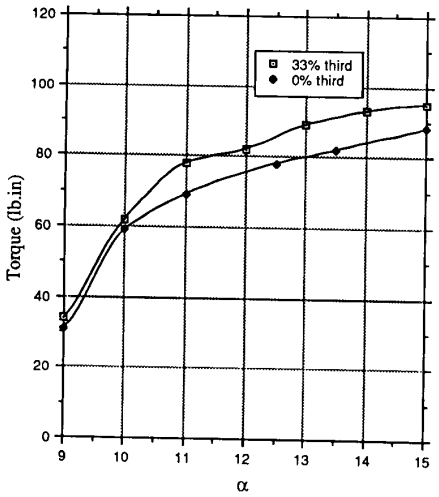

Fig. 25. Measured shaft torque under sinusoidal and combined fundamental and third-harmonic excitation.

Conclusion

An alternative topology for a SRM is proposed utilizing a five-phase current regulated PWM inverter. Linear analysis is used to search for an optimum pole arc and the required third harmonic of current to be added to the fundamental current waveform. These results have been backed by a more detailed analysis using the finite element approach and then by testing an actual motor. It was determined that an addition of 33% third harmonic results in 10% more torque even when saturation is properly taken into account. In addition, lower flux density in the air gap leaves room for having deeper slots and, consequently, more copper, resulting in a potential further improvement in future designs. Finally, the low torque ripple, due to smoothly rotating MMF in the airgap of this machine, compared with a switched reluctance machine, must be emphasized.

References

[1] P. J. Lawrenson, J. M. Stephenson, P. T. Blenkinsop, J. Corda, and N. N. Fulton, "Variable-speed switched reluctance motors," *Proc. Inst. Elect. Eng.*, vol. 127, pt. B, no. 4, pp. 253–265, July 1980.

[2] J. Byrne and J. C. Lacy, "Electrodynamic system comprising a variable reluctance machine" British Patent 1 321 110, 1970; U.S. Patent 3 956 678, May 11, 1976.

[3] L. Y. Xu and T. A. Lipo, "Analysis of a variable speed singly-salient reluctance motor utilizing only two transistor switches," *IEEE Trans. Industry Applications*, vol. 26, no. 2, pp. 229-236, Mar./Apr. 1990.
[4] J. S. Hsu, S. P. Liou, and H. H. Woodson, "Peak-MMF smooth-torque reluctance motors," *IEEE Trans. Energy Conv.*, vol. 5, no. 1, pp. 104-109, Mar. 1990.
[5] J. K. Kostko, "Polyphase reaction synchronous motors," *Amer. Inst. Elect. Eng.*, vol. 45, pp. 1162-1168, Nov. 1923.
[6] S. C. Rao, "Dynamic performance of reluctance motors with magnetically anisotropic rotors," *IEEE Trans. Power App. Syst.*, vol. PAS-95, no. 4, pp. 1369-1376, July/Aug. 1976.
[7] A. Vagati, "A reluctance motor drive for high dynamic performance applications," in *Conf. Rec. 1987 Ann. Mtg. IEEE Industry Applications Soc.*, pp. 295-302.
[8] T. A. Lipo, "Theory and control of synchronous machines," Class Notes, Univ. of Wisconsin-Madison, 1987.
[9] P. L. Alger, *The Nature of Induction Machines*. New York: Gordon and Breach, 1965.
[10] R. Schiferl, "Design considerations for salient pole permanent magnet synchronous motors in variable speed drive applications," Ph.D. thesis, Univ. Wisconsin-Madison, 1987.

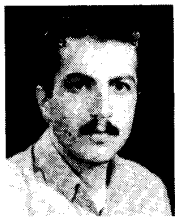

Hamid A. Toliyat was born in Mashhad, Iran, in 1957. He received the B.S. degree in 1982, the M.S. degree in 1986, and the Ph.D. degree in 1991 from Sharif University of Technology, Tehran, Iran, West Virginia University, Morgantown, WV, and the University of Wisconsin-Madison, respectively, all in electrical engineering.

Between 1982 and 1984, he worked for power companies in Iran. He is presently a post-doctoral fellow at the University of Wisconsin-Madison, where he is involved with converter-controlled ac machines.

Dr. Toliyat is a member of Sigma Xi.

Longya Xu was born in Hunan, China. He graduated from Shangtan Institute of Electrical Engineering in 1970. He received the B.E.E. degree from Hunan University, China, in 1982 and the M.S. and Ph.D. degrees from the University of Wisconsin, Madison, in 1986 and 1990.

From 1971-1978, he participated in 150-kvA synchronous machine design, manufacturing, and testing in China. From 1982-1984, he worked as a researcher for linear electric machines in the Institute of Electrical Engineering, Sinica Academia of China. Since he came to the United States, he has served as a consultant to several industry companies including Raytheon Co., US Wind Power Co., Pacific Scientific Co., and Unique Mobility Inc., and for various industrial concerns. He joined the Department of Electrical Engineering at the Ohio State University in 1990, where he is presently an Assistant Professor.

Dr. Xu received the 1990 First Prize Paper Award in the Industry Drive Committee. His research and teaching interests include dynamic modeling and converter-optimized design of electrical machines and drive systems.

Thomas A. Lipo (M'64-SM'71-F'87) received the B.E.E. and M.S.E.E. degrees from Marquette University, Milwaukee, WI, in 1962 and 1964, respectively, and the Ph.D. degree in electrical engineering from the University of Wisconsin in 1968. He was an NRC Postdoctoral Fellow at the University of Manchester Institute of Science and Technology, Manchester, England, from 1968 to 1969.

From 1969 to 1979, he was an Electrical Engineer in the Power Electronics Laboratory of Corporate Research and Development of the General Electric Company, Schenectady, NY. He became Professor of Electrical Engineering at Purdue University, Lafayette, IN, in 1979 and later joined the University of Wisconsin, Madison, in the same capacity. He has been involved in the research of power electronics and ac drives for over 25 years.

Dr. Lipo has received 11 IEEE prize paper awards including corecipient of the Best Paper Award in IEEE TRANSACTIONS ON INDUSTRY APPLICATIONS for 1984. In 1986, he received the Outstanding Achievement Award from the IEEE Industry Applications Society for his contributions to the field of ac drives.